IIETA International Information and Engineering Technology Association
Advancing the World of Information and Engineering

Mathematical Modelling of Engineering Problems
Vol. 12, No. 10, October, 2025, pp. 3468-3474
Journal homepage: http://iieta.org/journals/mmep

Thermomechanical Analysis of an Elastocaloric Cooler for Efficient Electronic Circuit Cooling

Luca Cirillo, Sabrina Gargiulo, Adriana Greco, Claudia Masselli, Vincenzo Orabona, Lucrezia Verneau*

Department of Industrial Engineering, University of Naples Federico II, Naples 80125, Italy

Corresponding Author Email: lucrezia.verneau@unina.it

https://doi.org/10.18280/mmep.121013

Received: 22 August 2025
Revised: 4 October 2025
Accepted: 10 October 2025
Available online: 31 October 2025

Keywords:
elastocaloric cooling, electronic circuits cooling, shape memory alloys, 2D numerical model, phase transformation, sustainable cooling

ABSTRACT

As electronic devices become increasingly powerful, the demand for efficient and sustainable cooling solutions has intensified. Traditional cooling methods, such as air and liquid cooling, face limitations in energy efficiency and scalability. The CHECK TEMPERATURE project explores an innovative approach to thermal management by leveraging elastocaloric technology for electronic circuit cooling. Elastocaloric cooling is based on the stress-induced phase transformation in shape memory alloys (SMAs) enabling highly efficient employment as solid-state refrigerants. The elastocaloric technology offers high thermal performance, compact design, and environmentally friendly operation, eliminating the need for conventional fluids refrigerants based on vapor compression. To evaluate its potential, a 2D numerical model of CHECK TEMPERATURE has been developed to analyze the energy performance of the system and simulate the elastocaloric effect in electronic cooling applications. The model provides insights into heat transfer dynamics, material behavior, and overall efficiency, guiding the optimization of elastocaloric cooling architectures. The elastocaloric effect shown by the binary Ni-Ti alloys has been also modelled, investigated and integrated into the 2D numerical tool. This contribution will cover theoretical modeling, numerical analysis, and analysis of the energy performance of elastocaloric cooling for electronic circuits. The results demonstrate the potential for a promising, scalable, and sustainable cooling technology, addressing the increasing thermal management challenges of next-generation electronics.

1. INTRODUCTION

Refrigeration and air conditioning systems account for a significant portion—estimated at more than 20%—of global energy consumption. The predominant technology employed in these systems is based on Vapor Compression (VC), which, despite its historical success and wide adoption, faces increasing criticism due to two major limitations. First, the refrigerants used in VC systems often have high Global Warming Potentials (GWP), contributing significantly to climate change. Second, these systems have reached a plateau in performance, limiting further gains in energy efficiency [1].

The urgency to reduce environmental impact and improve energy efficiency has prompted the scientific and engineering communities to explore alternative refrigeration technologies. Among these, Not-In-Kind (NIK) refrigeration technologies have emerged as promising contenders [2]. NIK systems deviate from traditional vapor compression cycles and instead leverage physical phenomena such as the caloric effects found in specific solid-state materials [3]. These effects—manifesting as temperature changes under varying external fields (magnetic, electric, or mechanical)—form the basis for magnetocaloric, electrocaloric, and mechanocaloric refrigeration systems [4].

Of these solid-state cooling technologies, elastocaloric cooling has garnered increasing attention for its potential to offer efficient, compact, and environmentally benign refrigeration [5]. The elastocaloric effect (eCE) arises when a mechanical stress—typically tensile or compressive—is applied to a Shape Memory Alloy (SMA), triggering a solid-state phase transformation between austenite and martensite phases [6]. This transformation is associated with significant thermal effects: exothermic heating during loading and endothermic cooling during unloading. Key equations govern this behavior in terms of isothermal entropy change (ΔS) and adiabatic temperature change (ΔT_{ad}), with material-specific properties such as latent heat, transformation strain, critical stress, and thermal hysteresis playing pivotal roles in overall performance:

$$\Delta S = \int_{\sigma_0}^{\sigma_1} \left(\frac{\partial \varepsilon}{\partial T}\right)_{\sigma} d\sigma \quad (1)$$

$$\Delta T_{ad} = -\int_{\sigma_0}^{\sigma_1} \frac{T}{C}\left(\frac{\partial \varepsilon}{\partial T}\right)_{\sigma} d\sigma \quad (2)$$

Shape memory alloys, particularly those based on binary NiTi compositions, have proven to be excellent candidates for elastocaloric applications. These materials exhibit substantial

adiabatic temperature changes (ΔT_{ad} up to 25 K), high latent heat during transformation, and significant entropy changes. The transformation behavior can be tuned through alloying and thermomechanical treatment, and their fatigue life can exceed 10^7 cycles under optimized conditions.

Despite their potential, elastocaloric technologies is a promising frontier that remains underexplored in practical implementations. Most of the devices investigated to date are proof-of-concept models aimed at room-scale air conditioning. Most utilize tensile loading mechanisms due to their simplicity and historical precedence [7]. Notable developments include the early work by Cui et al. [8], who introduced a rotating device employing NiTi wires, and subsequent advances by Kirsch et al. [9] using cam-driven loading in a rotary prototype.

Alternative loading strategies such as compression and bending have shown potential to mitigate some of these limitations. Bending, in particular, may reduce mechanical dissipation and localized stress concentrations, extending the operational life of the material. However, such configurations have been tested only in a limited number of studies, typically at micro-scale or with reduced cooling capacities [10, 11].

Furthermore, existing elastocaloric devices have largely targeted macro-scale applications. There has been minimal focus on applications within microelectronics—a domain that faces pressing thermal management challenges due to increasing device density and power consumption. Current conventional cooling methods, including forced convection and phase-change cooling, are often inadequate to handle the high heat fluxes generated by modern microchips and sensors.

This study addresses the aforementioned research gap by presenting a novel elastocaloric device concept specifically designed for electronic circuits cooling. Unlike previous studies, the device is optimized for compactness and thermal performance in high heat flux environments. Two configurations are proposed and compared: one employing tensile loading and the other using mechanical bending.

To the best of the authors' knowledge, this is the first investigation to integrate bending-mode elastocaloric activation within an Active elastocaloric Regenerator (AeR) cycle for electronics cooling. The comparison is conducted using a two-dimensional finite element model that captures the thermal and mechanical dynamics of the system. Performance metrics such as temperature span, cooling power, and coefficient of performance (COP) are evaluated under varying operating conditions.

This work contributes to the expanding field of solid-state refrigeration by introducing a scalable, efficient, and application-specific elastocaloric cooling solution, paving the way for environmentally responsible and high-performance thermal management in next-generation electronics.

2. SYSTEM DESIGN AND CONFIGURATION

This work introduces two elastocaloric cooling system configurations designed for electronic applications, namely a bending-based and a tensile-based prototype as visible in Figure 1. Both systems utilize $Ni_{50.8}Ti_{49.2}$ shape memory alloy wires as the active cooling medium and air as the Heat Transfer Fluid (HTF).

The bending-mode configuration comprises two stacked microchannels, each containing arrays of NiTi wires. The core mechanism is a central oscillating plate that cyclically deflects upward and downward, inducing mechanical bending in the wires located in either channel. The air passes through these channels in counterflow during alternating thermal phases, thereby promoting effective heat exchange. This architecture benefits from faster heat cycling due to the simultaneous operation of the upper and lower wire sets during different AeR cycle phases.

In the tensile design, the elastocaloric wires are mounted in two parallel beds and loaded axially via a piston-driven support mechanism. This setup allows for symmetric stress application and partial energy recovery, as the unloading of one bed assists the loading of the other. The air flows through each bed in a direction coordinated with the thermal phase of the wires. Although this configuration offers robust thermal gradients, it requires more complex mechanical actuation.

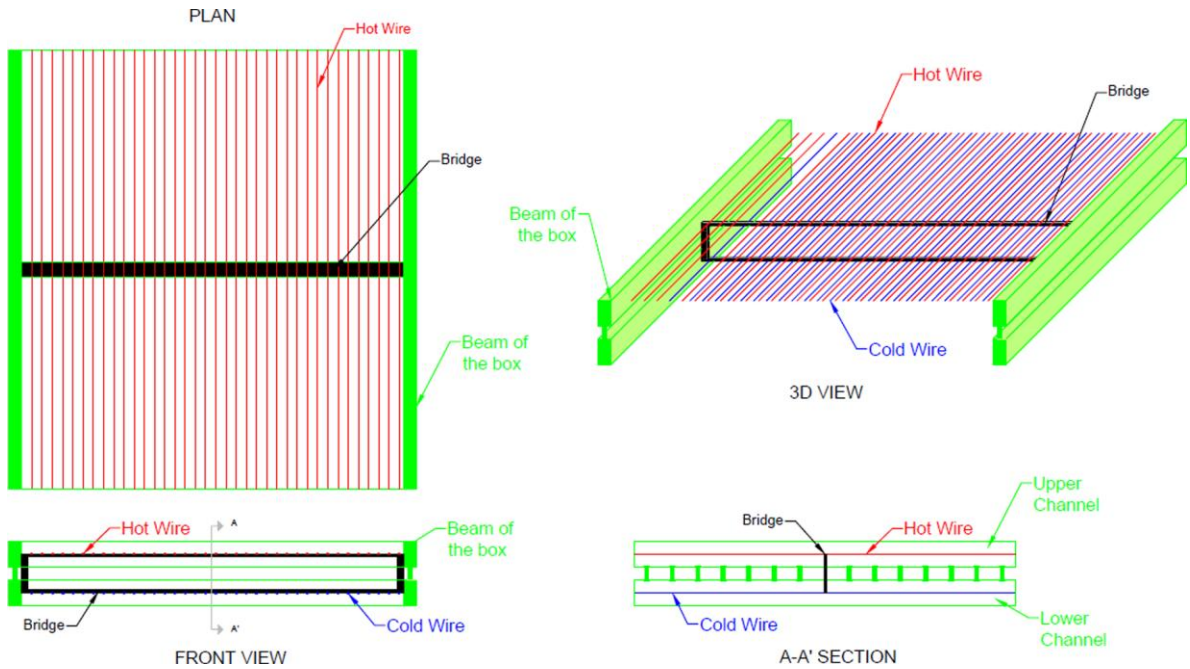

(a) Bending

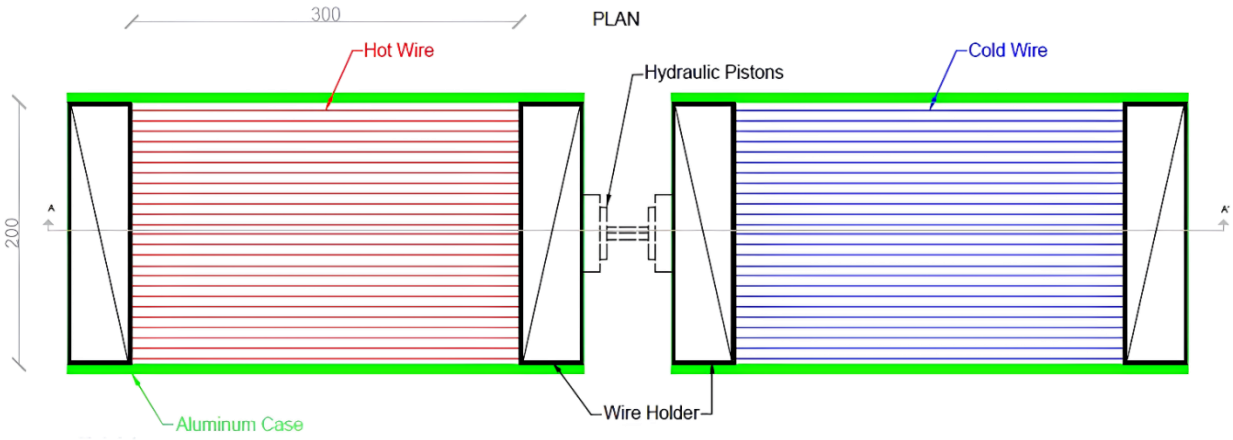

(b) Tensile

Figure 1. Layouts of system configurations

Both prototypes incorporate a common hydraulic loop, consisting of dual fans, insulated galvanized steel ducting, and electronic control valves. Motorized dampers regulate airflow distribution, while embedded thermocouples and Resistance Temperature Detector (RTD) sensors track temperature profiles. Additional instrumentation includes anemometers and pressure sensors for fluid dynamics analysis. To simulate a realistic electronic thermal load, a resistive heating element is attached to the target cooling surface.

3. NUMERICAL MODELING APPROACH

A two-dimensional (2D) Finite Element Method (FEM) model was implemented in COMSOL Multiphysics to simulate the thermal behavior and energetic performance of the two configurations. The model simulates a full AeR cycle: loading, heat rejection, unloading, and heat absorption.

3.1 Governing physics and boundary conditions

The model solves the coupled Navier-Stokes, energy, and phase transition equations for both air and the elastocaloric wires. Airflow is considered incompressible and adiabatic, with negligible viscous dissipation:

$$\begin{cases} \dfrac{\partial u}{\partial x}+\dfrac{\partial v}{\partial y}=0 \\ \dfrac{\partial u}{\partial t}+u\dfrac{\partial u}{\partial x}+v\dfrac{\partial u}{\partial y}=-\dfrac{1}{\rho_{air}}\dfrac{\partial p}{\partial x}+\nu\left(\dfrac{\partial^2 u}{\partial x^2}+\dfrac{\partial^2 u}{\partial y^2}\right) \\ \dfrac{\partial v}{\partial t}+u\dfrac{\partial v}{\partial x}+v\dfrac{\partial v}{\partial y}=-\dfrac{1}{\rho_{air}}\dfrac{\partial p}{\partial y}+\nu\left(\dfrac{\partial^2 v}{\partial x^2}+\dfrac{\partial^2 v}{\partial y^2}\right) \\ \dfrac{\partial T_{air}}{\partial t}+u\dfrac{\partial T_{air}}{\partial x}+v\dfrac{\partial T_{air}}{\partial y}=\dfrac{k_{air}}{\rho_{air}c_{air,p}}\left(\dfrac{\partial^2 T_{air}}{\partial x^2}+\dfrac{\partial^2 T_{air}}{\partial y^2}\right) \\ \rho_{SMA}c_{SMA,p}\dfrac{\partial T_{SMA}}{\partial t}=k_{SMA}\left(\dfrac{\partial^2 T_{SMA}}{\partial x^2}+\dfrac{\partial^2 T_{SMA}}{\partial y^2}\right)+g''' \end{cases} \tag{3}$$

Heat generation in the SMA wires is captured through transient source terms that model latent heat effects and mechanical work input:

$$g''' = \frac{\rho c \Delta T(\xi)}{t_{load}} \tag{4}$$

where, ΔT has been evaluated through the Lagoudas Model [12]:

$$\Delta T_{ad}(\xi) = -\frac{\dfrac{\xi\rho b^M - \sigma H - \frac{1}{2}\Delta SM_s}{\rho\Delta s_0}\left(\alpha^A+\xi(\alpha^M-\alpha^A)\right)-\left[\dfrac{Hsgn(\sigma)+\Delta S\sigma}{\rho\Delta s_0(M_s-M_f)}\left(-Y+\xi b^M\rho-\sigma H-\frac{1}{2}\Delta S\sigma^2+\rho\Delta SM_s\right)\right]}{\rho c-\left[\dfrac{\rho\Delta s_0}{\rho\Delta s_0(M_s-M_f)}\left(-Y+\xi b^M\rho-\sigma H-\frac{1}{2}\Delta s\sigma^2+\rho\Delta SM_s\right)\right]}\Delta\sigma \tag{5}$$

The thermal hysteresis of the SMA is considered by adopting different values of latent heat for loading and unloading, as well as the work required [13]. According to Tušek et al. [14], it is possible to estimate the net-work as the area enclosed by the hysteresis cycle defined by the transformations in s-T plane as:

$$w_{net} = w_{load} - w_{unload} \tag{6}$$

The kinetics of the martensitic transformation are modeled using phase fraction rate equations from Qian et al. [15], incorporating transformation probabilities dependent on stress and temperature.

The martensite volume fraction $\dot{\xi}_M$ is evaluated through the Eq. (6):

$$\dot{\xi}_M = -\xi_M\psi^{MA}(T_{SMA},\sigma)+\xi_A\psi^{AM}(T_{SMA},\sigma) \tag{7}$$

during the A-M and the M-A transformations:

$$\xi_A+\xi_M=1 \tag{8}$$

The transition probabilities ψ^{MA} and ψ^{AM} are calculated through the approach proposed by Qian et al. [15]:

$$\psi^{AM}(T_{SMA},\sigma) = \frac{1}{\theta}\frac{\exp\left(-a\left(\dfrac{\sigma_{AM}(T_{SMA})-\sigma}{E_A}\right)^2\right)}{\mathrm{erf}\left(\sqrt{a}\dfrac{\sigma_{AM}(T_{SMA})-\sigma}{E_A}\right)+\mathrm{erf}\left(\sqrt{a}\dfrac{\sigma_{AM}(T_{SMA})+\sigma}{E_A}\right)} \tag{9}$$

$$\psi^{MA}(T_{SMA},\sigma)=\frac{1}{\theta}\frac{\exp\left(-b\left(\frac{\sigma_{MA}(T_{SMA})-\sigma}{E_M}\right)^2\right)}{\operatorname{erfc}\left(\sqrt{b}\frac{\sigma_{MA}(T_{SMA})-\sigma}{E_M}\right)} \quad (10)$$

where:

$$a=\frac{E_A V_{SMA}}{2BT_{SMA}} \quad (11)$$

$$b=\frac{E_M V_{SMA}}{2BT_{SMA}} \quad (12)$$

Boundary conditions include a fixed air inlet temperature (293 K), controlled inlet velocities (3–11 m/s), and thermally insulated outer surfaces. The model captures heat transfer during both during mechanical actuation and airflow stages.

3.2 Material properties and kinetics

The employed SMA is $Ni_{50.8}Ti_{49.2}$ [16] subjected to treatments that ensure a longer fatigue-life. An 8% strain with a strain rate of 0.025 s^{-1} is considered for loading/unloading cycles. A 0.2 s time of loading/unloading is selected, so the transformation can be considered as adiabatic.

$Ni_{50.8}Ti_{49.2}$ wires are modeled with a thermal conductivity of 15 W/mK, specific heat of 550 J/kgK, and density of 6500 kg/m³. Latent heat and transformation hysteresis differ between tensile and bending configurations.

3.3 Mesh and solver configuration

Mesh independence, the solution's independence from the spatial grid was examined by conducting simulations using several grids under identical initial, boundary, and operational conditions. The evaluated grids consisted of: sparse (comprising 81,218 volumetric triangular elements), normal (containing 137,084 elements), and dense (including 384,424 volumetric elements). Regarding the temperature profiles in the last phase of the AeR cycle, we observed a strong correlation between the solutions for 137084 and 384424, with a maximum divergence in air temperatures of less than 0.03 K. Consequently, to reduce calculation time, we have opted to utilise a standard grid including 137,084 volumetric triangular pieces. Final simulations used the "normal" mesh for computational efficiency. Time integration was conducted using a BDF solver, and simulations continued until thermal cyclic steady state was achieved.

4. VALIDATION AND EXPERIMENTAL CORRELATION

To ensure model accuracy, validation was performed using experimental data from a campaign involving trained NiTi wires subjected to rapid loading and unloading. Temperature variations were recorded using an infrared camera system, and results were compared with a simplified 1D MATLAB-based simulation. The experimental setup involved tensile loading of NiTi wires using an Instron test bench, with stress ramps up to 550 MPa at 0.2 s^{-1} strain rates. The temperature evolution observed during stress cycling matched the model predictions within a 1°C deviation. This confirmed that the phase transformation kinetics and elastocaloric behavior were accurately captured. Further details are reported by Cirillo et al. [17].

5. RESULTS AND DISCUSSION

Simulations were conducted for both prototypes over a range of airflow velocities and heat exchange durations. Key performance metrics include the temperature span (ΔT_{span}), cooling power, and COP:

$$\Delta T_{span}=\left(T_{env}-\frac{1}{t_{cycle}}\int_{0+n\,t_{cycle}}^{t_{cycle}+n\,t_{cycle}}T_{air,outlet}(t)dt\right) \quad (13)$$

$$\dot{Q}_{ref}=\int_{t_{load}+\,t_{fluid}+\,t_{unload}+n\,t_{cycle}}^{t_{cycle}+n\,t_{cycle}}\dot{m}_{air}c_{air}\left(T_{env}-T_{air,outlet}(t)\right)dt \quad (14)$$

$$COP=\frac{\dot{Q_{ref}}}{\dot{W}} \quad (15)$$

Figures 2 illustrate the temperature range over time for fluid flow, parameterised by air velocity for the two geometries: (a) tensile and (b) bending. Figure 3 illustrates the cooling power as a function of fluid blow duration, parameterised by fluid velocity for both configurations: (a) tensile and (b) bending. Figure 4 presents the COP as a function of air velocity, parameterised by blown duration for both architectures: (a) tensile and (b) bending.

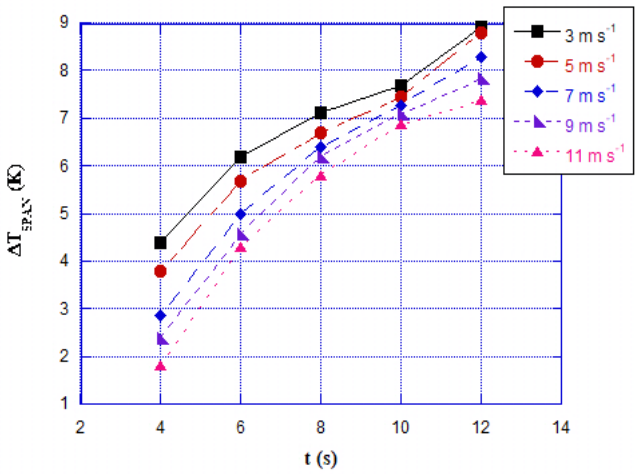

(a)

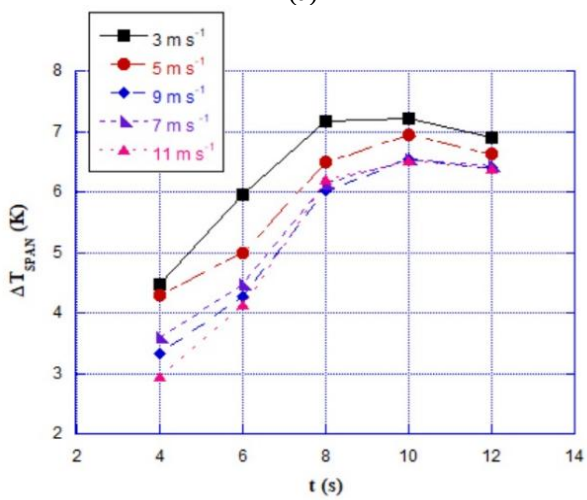

(b)

Figure 2. Temperature variation over time for fluid flow parameterised by air velocity: (a) tensile load; (b) bending

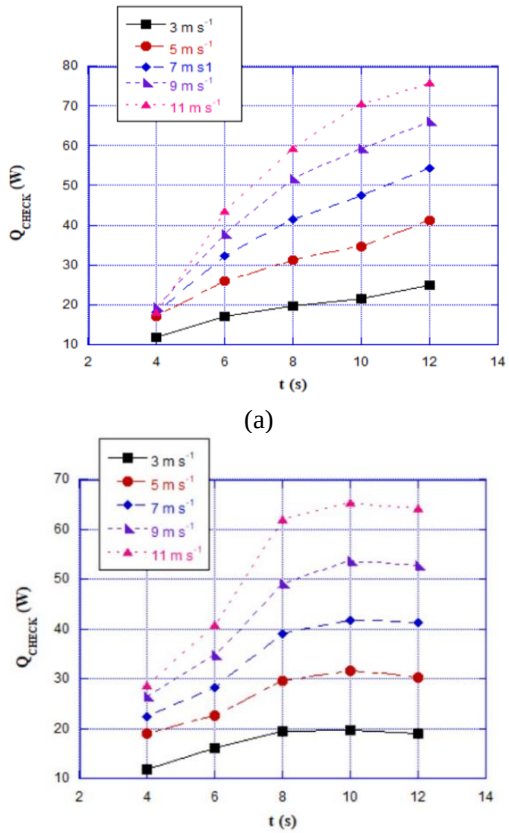

Figure 3. Cooling power as a function of time for fluid flow, parameterised by air velocity: (a) tensile load; (b) bending

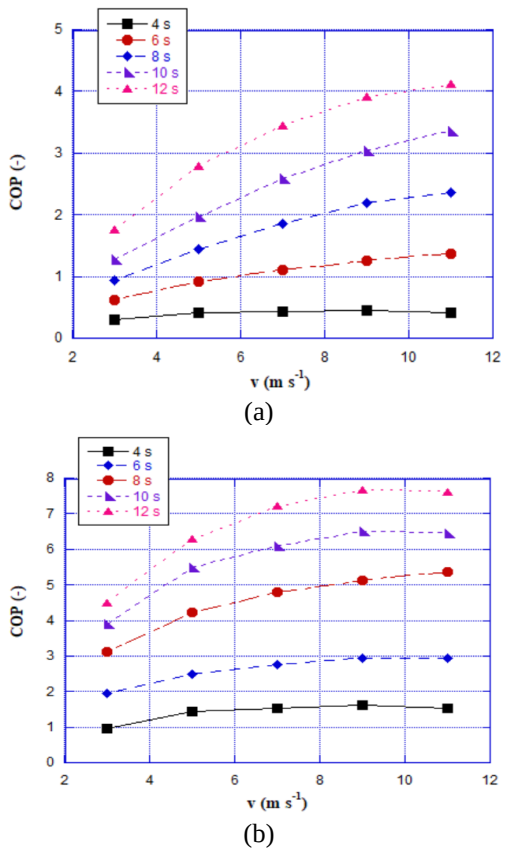

Figure 4. Coefficient of performance versus time for fluid flow parameterised by air velocity: (a) tensile load; (b) bending

At shorter fluid interaction times (4–6 s), both configurations yielded similar ΔT_{span}. However, at longer durations (up to 12 s), the tensile setup demonstrated higher ΔT_{span}, reaching up to 9 K compared to 7.2 K for the bending setup. This advantage arises from the larger adiabatic temperature change achievable with tensile loading. Cooling power increased with airflow velocity due to greater mass flow, peaking at 76 W for the tensile setup and 65 W for bending. However, performance declined when fluid flow time exceeded optimal durations, especially for bending due to thermal saturation. While the tensile prototype achieved higher ΔT_{span}, the bending configuration consistently outperformed in terms of COP, reaching a maximum of 7.7. This reflects its lower mechanical energy input requirement, enhancing system-level efficiency.

6. CONCLUSIONS

This study presents a novel elastocaloric cooling concept tailored for electronics. A comparison between tensile and bending configurations was conducted using validated FEM simulations.

The following conclusions can be drawn:

- bending yields superior COP due to reduced mechanical input.
- Tensile achieves higher ΔT_{span} and cooling power, albeit with greater actuation energy cost.
- Optimal performance conditions differ for each configuration, highlighting trade-offs between thermal gradient and efficiency.

The findings affirm the viability of elastocaloric cooling in compact electronics and encourage for further development of bending-based AeR systems.

ACKNOWLEDGMENT

The paper is an outcome of the project CHECK TEMPERATURE that is financially supported by the 2021 internal grant reserved for Fixed-Term Research of Department of Industrial Engineering, University of Naples Federico II.

REFERENCES

[1] Cen, J., Zeng, L., Liu, X., Wang, F., Deng, S., Yu, Z., Zhang, G.M., Wang, W. (2024). Research on energy-saving optimization method for central air conditioning system based on multi-strategy improved sparrow search algorithm. International Journal of Refrigeration, 160: 263-274. https://doi.org/10.1016/j.ijrefrig.2024.01.012

[2] Bansal, P., Vineyard, E., Abdelaziz, O. (2012). Status of not-in-kind refrigeration technologies for household space conditioning, water heating and food refrigeration. International Journal of Sustainable Built Environment, 1(1): 85-101. https://doi.org/10.1016/j.ijsbe.2012.07.003

[3] Qian, S., Takeuchi, I. (2024). Sizing up caloric devices. Science, 385(6708): 493-494. https://doi.org/10.1126/science.adp371

[4] Xu, X., Xie, W.F., Li, F.B., Niu, C., Li, M., Wang, H. (2024). General approach for efficient prediction of refrigeration performance in caloric materials. Physical

Review Applied, 22(1): 014036. https://doi.org/10.1103/PhysRevApplied.22.014036
[5] Mevada, H., Liu, B., Gao, L., Hwang, Y., Takeuchi, I., Radermacher, R. (2024). Elastocaloric cooling: A pathway towards future cooling technology. International Journal of Refrigeration, 162: 86-98. https://doi.org/10.1016/j.ijrefrig.2024.03.014
[6] Mañosa, L., Planes, A. (2024). Elastocaloric effect in shape-memory alloys. Shape Memory and Superelasticity, 10: 89-98. https://doi.org/10.1007/s40830-024-00477-x
[7] Cui, J. (2024). Early efforts on elastocaloric cooling (2002 to 2014). Shape Memory and Superelasticity, 10: 80-88. https://doi.org/10.1007/s40830-024-00475-z
[8] Cui, J., Wu, Y.M., Muehlbauer, J., Hwang, Y., Radermacher, R., Fackler, S., Wuttig, M., Takeuchi, I. (2012). Demonstration of high efficiency elastocaloric cooling with large ΔT using NiTi wires. Applied Physics Letters, 101(7): 073904. https://doi.org/10.1063/1.4746257
[9] Kirsch, S.M., Welsch, F., Michaelis, N., Schmidt, M., Wieczorek, A., Frenzel, J., Eggeler, G., Schütze, A., Seelecke, S. (2018). NiTi-based elastocaloric cooling on the macroscale: From basic concepts to realization. Energy Technology, 6(8): 1567-1587. https://doi.org/10.1002/ente.201800135
[10] Sharar, D.J., Radice, J., Warzoha, R., Hanrahan, B., Smith, A. (2021). Low-force elastocaloric refrigeration via bending. Applied Physics Letters, 118(18): 183903. https://doi.org/10.1063/5.0041500
[11] Cheng, S.Y., Sun, W.J., Li, X.S., Zhang, J.J. (2024). Elastocaloric effect and cooling performance of NiTi sheets in a continuous rotating bending elastocaloric cooler. APL Materials, 12: 081108. https://doi.org/10.1063/5.0217563
[12] Lagoudas, D., Hartl, D., Chemisky, Y., Machado, L., Popov, P. (2012). Constitutive model for the numerical analysis of phase transformation in polycrystalline shape memory alloys. International Journal of Plasticity, 32: 155-183. https://doi.org/10.1016/j.ijplas.2011.10.009
[13] Ossmer, H., Lambrecht, F., Gültig, M., Chluba, C., Quandt, E., Kohl, M. (2014). Evolution of temperature profiles in TiNi films for elastocaloric cooling. Acta Materialia, 81: 9-20. https://doi.org/10.1016/j.actamat.2014.08.006
[14] Tušek, J., Engelbrecht, K., Mañosa, L., Vives, E., Pryds, N. (2016). Understanding the thermodynamic properties of the elastocaloric effect through experimentation and modelling. Shape Memory and Superelasticity, 2(4): 317-329. https://doi.org/10.1007/s40830-016-0094-8
[15] Qian, S.X., Yuan, L.F., Yu, J.L., Yan, G. (2017). Numerical modelling of an active elastocaloric regenerator refrigerator with phase transformation kinetics and the matching principle for materials selection. Energy, 141: 744-756. https://doi.org/10.1016/j.energy.2017.09.116
[16] Zhou, M., Li, Y.S., Zhang, C., Li, S.J., Wu, E., Li, W., Li, L.F. (2018). The elastocaloric effect of Ni50.8Ti49.2 shape memory alloys. Journal of Physics D: Applied Physics, 51(13): 135303. https://doi.org/10.1088/1361-6463/aaafc2
[17] Cirillo, L., Greco, A., Masselli, C. (2022). CHECK TEMPERATURE: A small-scale elastocaloric device for the cooling of the electronic circuits. International Journal of Heat and Technology, 40(3): 665-670. https://doi.org/10.18280/ijht.400302

NOMENCLATURE

Roman symbols

A	Austenite phase temperature, K
AeR	Active elastocaloric regenerator
a	Grouping factor
B	Boltzmann constant, $m^2 \cdot kg \cdot s^{-2} \cdot K^{-1}$
b	Grouping factor
c	Specific heat capacity, $J \cdot kg^{-1} \cdot K^{-1}$
COP	Coefficient of performance
E	Young modulus, MPa
f	Frequency, Hz
FEM	Finite Element Method
g	Elastocaloric term, $W \cdot m^{-3}$
GWP	Global Warming Potential
H	Latent heat, $J \cdot g^{-1}$
HTF	Heat Transfer Fluid
k	Thermal conductivity, $W \cdot m^{-1} \cdot K^{-1}$
M	Martensite phase temperature, K
$\dot{m}$	Flow rate, $kg \cdot s^{-1}$
n	Number of times
p	Pressure, Pa
$\dot{Q}$	Cooling power, W
S	Entropy, J·kg·K
SMA	Shape Memory Alloy
T	Temperature, K
t	Time, s
u	x-velocity field component, $m \cdot s^{-1}$
v	y-velocity field component, $m \cdot s^{-1}$
VC	Vapor Compression
w	Loading/unloading work, $J \cdot g^{-1}$
x	Longitudinal spatial coordinate, m
y	Orthogonal spatial coordinate, m

Greek symbols

Δ	Finite difference
ε	Strain, N
θ	Relaxation time constant for martensitic phase transformation [s]
υ	Cinematic viscosity, $m^2 \cdot s^{-1}$
ξ	Phase fraction, -
$\dot{\xi}$	Instantaneous phase fraction, s^{-1}
ρ	Density, $kg \cdot m^{-3}$
σ	Uniaxial stress, MPa
ψ	Probability, -

Subscripts

0	Initial
1	Final
A	Austenitic
AM	Austenite-to-Martensite transformation
ad	Adiabatic
air	Air
CHANNEL	On the single channel
CHECK	On the whole device
cool	Cooling
cycle	Cycle

env	Environment	outlet	Outlet
f	Finish	p	Constant pressure
fluid	Fluid	ref	Refrigeration
load	Loading	s	Start
M	Martensitic	SMA	Shape Memory Alloy
MA	Martensite-to-Austenite transformation	span	Span
net	Net	unload	Unloading